The critical ventilation velocity for transverse double fires in tunnel

Q. Zhang[a], G. Pei[b]*
[a] *School of Civil Engineering and Architecture, Southwest Petroleum University, Chengdu, China*
[b] *School of Architectural Economics and Engineering Management, Hubei Business College, Wuhan, China*
* E-mail: 570769297@qq.com

Abstract. The critical velocity of longitudinal ventilation is one of the most important parameters in tunnel fires. Most previous studies simulated fire scenarios in which only one fire source exists in the tunnel. However, the critical velocity will change under the condition of transverse double fires. In this study, the critical ventilation velocity under the transverse double-fire condition compared with the single fire source was analyzed by using the Fire Dynamics Simulator (FDS). The results show that the smoke movement for transverse double fires in the tunnel is affected by both the buoyant force and the shear stress of the sidewalls. As the distance between the double fires increases, the critical velocity decreases first, then increases and eventually decreases. When the double fire sources are both near the side walls, the critical velocity is approximately equal to the critical velocity for adjacent double fires at the center. Finally, relations between the influence coefficient of distance and the dimensionless transverse distance as well as correlations between the critical ventilation velocity with and without distances for double fires were developed. The presented correlation can provide reference value for smoke control and personnel evacuation in case of tunnel fires.

1. Introduction

In recent years, various railway tunnel, highway tunnel, and urban subway projects have been rapidly developed worldwide [1]. Fire safety is significantly important, particularly in tunnels. Many fire investigations have shown that the most dangerous factor leading to casualties is not the high temperature of the fire but the smoke produced by the fire, so smoke flow has a significant impact on fire-fighting strategy and personnel evacuation. The method of emergency plan and smoke control most currently applied in many tunnels is based on longitudinal ventilation produced mechanically [2]. The critical ventilation velocity is the minimum ventilation velocity that could force the smoke to stay at downstream of the fire source only. When ventilation velocity below the critical velocity is not sufficient to prevent the smoke from spreading against the direction of longitudinal ventilation air, the back-layering phenomenon (smoke back-layering length) will appear in the fire upstream, which is not conducive for personnel evacuation [3]. Therefore, one of the foremost parameters for managing the smoke movement effectively is the value of critical velocity.

The characteristics of smoke movement were studied by the earliest tunnel fire tests conducted in Switzerland. Subsequently, a series of large-scale fire experiments established in nine Western countries showed that smoke flow strongly depends on the ventilation velocity [4]. Currently, several different formulas to predict the critical velocity are developed by a theory based on the Froude number, and some scholars note that Thomas [5] was one of the first to engage in this study and set up the prediction determination for the critical velocity. The relationship between critical velocity and heat release rate was developed as

$$V_c = \left(\frac{gQH}{\rho_0 C_p T_f A} \right)^{1/3},$$ (1)

where Q is the heat release rate, W;

V_c is the critical velocity, m/s; g is the acceleration of gravity, m/s²;

H is the tunnel height, m;

ρ_0 is the air density, kg/m³;

C_p is the specific heat at constant pressure, J/kg·K;

T_f is the hot air temperature, K;

A is the cross-sectional area of the tunnel, m².

According to the dimension analysis, Oka and Athinson [6], Wu and Bakar [7], and Li et al. [8] proposed different prediction models for critical ventilation velocity. In terms of small-scale experimentation, Oka and Athinson [6] found that the critical velocity does not increase with the one-third power of the heat release rate with a high value, therefore, a new formula was established in dimensionless form through correlation of experimental results:

$$V_c^* = \begin{cases} K_v \left(\dfrac{Q^*}{0.12} \right)^{1/3} & Q^* \leq 0.12, \\ K_v & Q^* > 0.12, \end{cases} \tag{2}$$

where $Q^* = Q / c_p \rho_0 T_a g^{1/2} H^{5/2}$,

$V^* = V / \sqrt{gH}$,

K_v is a constant value ranging from 0.22 to 0.38,

T_a is the ambient temperature, K.

Wu and Bakar [7] studied, by experiment and numerical simulation, the influence of different cross-section shapes on the critical ventilation velocity. From the model by Oka and Athinson [6], a new prediction model was expressed with the tunnel hydraulic height:

$$V_c^\bullet = \begin{cases} 0.4 \left(\dfrac{Q^\bullet}{0.2} \right)^{1/3} & Q^* \leq 0.2, \\ 0.4 & Q^* > 0.2, \end{cases} \tag{3}$$

where $Q^* = Q / c_p \rho_0 T_a g^{1/2} \overline{H}^{5/2}$,

$V^* = V / \sqrt{g\overline{H}}$,

$\overline{H}$ is the tunnel hydraulic height, m.

Li et al. [8] carried out a series of small-scale experiments in two tunnels of 12 m length with diverse cross-sections to investigate the critical velocity, their prediction model is given as

$$V_c^\bullet = \begin{cases} 0.81 Q^{*1/3} & Q^* \leq 0.15, \\ 0.43 & Q^* > 0.15, \end{cases} \tag{4}$$

where $Q^* = Q / c_p \rho_0 T_a g^{1/2} H^{5/2}$,

$V^* = V / \sqrt{gH}$.

In addition to the factor of cross-section shape, other elements, such as blockage and slope, also affect the critical velocity in a tunnel. Some authors have reported that the critical velocity decreases because of vehicle blockage [9–11]. Alva et al. [12] noted that the relative position between the fire source and blockage can increase the critical velocity compared with that of the same situation without vehicular blockage. For four slope values (0°, 3°, 6°, and 9°), Chow et al. [13] showed that the critical velocity for sloped tunnels is higher than that for horizontal tunnels. Yi et al. [14] suggested that the critical velocity decreases as slope value ranging from −3 % to 3 % increases gradually. In these studies, fires were always set on the centerline in the tunnel, but in reality, a fire can

happen at any location in the transverse direction of tunnel. A "mirror" effect was considered by Hu et al. [15] to derive the ratio of the critical velocity for a fire next to a sidewall to that for a fire in the middle by theoretical analysis, the ratio value was estimated as 1.26. Furthermore, Zhong et al. [16] noted that the critical velocity would increase exponentially with decreasing distance between the fire and the sidewall. Wang et al. [17] revealed, using tunnel height as the characteristic length, that the critical velocity for a fire near a wall is distinctly higher than that for fire at other positions in the lateral direction, and the ratio is approximately equal to 1.2.

These previous studies have always focused on a single fire in the tunnel. In fact, under the congestion conditions caused by tunnel fire, a burning vehicle could easily ignite adjacent vehicles when the heat radiation grows adequately, at the same time, the critical velocity is influenced by the greater heat release rate and the distance between fire sources. Therefore, in this study, different conditions established by numerical simulation were used to investigate the critical velocity.

2. Methods

2.1. Physical model

In this study, a tunnel model measuring 15×1×0.25 m was established by using Fire Dynamics Simulator (FDS) version 6.6.0, as shown in Figure 1. The tunnel structure, including walls, ceiling, and floor, was modelled as concrete with thermal thickness, their boundary conditions were set to "CONCRETE" and the thermal properties of concrete were specified by the "MATL" command in FDS. The velocity at the walls, ceiling, and floor was assumed to be the default conditions by FDS. Two surfaces, including a portal set to "SUPPLY" and an exit called "OPEN" in FDS, were placed at both ends of the model tunnel, the longitudinal ventilation velocity was specified at the portal surface to introduce the air flow to the tunnel entry, and the open surface was connected with the atmospheric environment. The ambient temperature was 293 K and the atmospheric pressure was 101,325 Pa. The heat release rate was assigned as the heat release rate per unit area by using the "HRRPUA" command in FDS. The smoke produced by the burnable methane (CH_4) was used to model soot. Two identical rectangular fire sources were symmetrically placed on the floor of the tunnel center and horizontally moved to the sidewalls. In this study, X, Y, and Z represent the longitudinal, transverse, and vertical directions, respectively. All combinations are listed in Table 1.
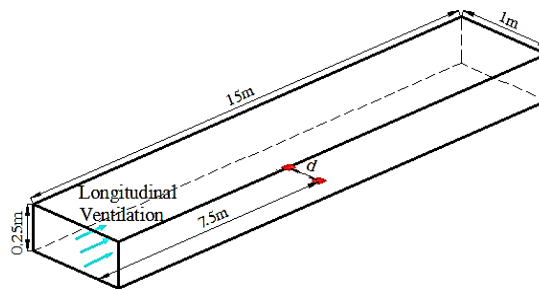

Figure 1. Diagram of the model tunnel.

Table 1. Relative position of transverse double fires.

Fire combination	Relative position of fire, m						
3 + 3 kW	0.1	0.2	0.3	0.4	0.5	0.6	0.7
6 + 6 kW	0.1	0.2	0.3	0.4	0.5	0.6	0.7
7.5 + 7.5 kW	0.1	0.2	0.3	0.4	0.5	0.6	0.7
12 + 12 kW	0.1	0.2	0.3	0.4	0.5	0.6	0.7

2.2. Large-eddy simulation

FDS is a computational fluid dynamics (CFD) model of fire-driven fluid flow to numerically solve a modality of the Navier-Stokes equations fit for speed with a low Mach number and smoke and heat transport by thermally-driven flow [18, 19]. The default combustion model used in the simulation was mix-controlled with infinitely fast chemistry. The turbulence model has four available models, including Deardorff, Vreman, constant Smagorinsky, and dynamic Smagorinsky for the subgrid-scale (sgs) turbulent viscosity [20], the default Deardorff model was applied in the simulation.

The default Deardorff turbulent viscosity is expressed as

$$(\mu_{LES} / \rho) = C_v \Delta \sqrt{k_{sgs}}, \tag{5}$$

where $C_v = 0.1$ and the sgs kinetic energy is taken from an algebraic relationship based on scale similarity [18, 19]. The filter width of Large-eddy simulation is taken as the geometric mean of the local mesh spacing in each direction,

$$\Delta = (\delta x \delta y \delta z)^{(1/3)},$$

where δx, δy, and δz are the dimensions of the smallest cell.

The thermal conductivity and material diffusivity are related to the turbulent viscosity by

$$k_{LES} = \frac{\mu_{LES} c_p}{Pr_t}; \tag{6}$$

$$(\rho D)_{LES} = \frac{\mu_{LES}}{Sc_t}. \tag{7}$$

The turbulent Prandtl number Pr_t and the turbulent Schmidt number Sc_t are assumed to be constant for a given scenario. The Pr_t and Sc_t have constant default values of 0.5, which can better simulate the fire smoke flow [11].

2.3. Grid independence test

Double fires (6 + 6 kw) at a distance of 0.1 m, as an example, were employed to test the grid independence. The grid region was divided into a left part (L) from 0 to 6 m, a middle part (M) from 6 to 9 m, and a right part (R) from 9 to 15 m in the x direction. The temperature measured under the tunnel ceiling was selected as the test parameter, and the longitudinal ventilation velocity was set to 0.35 m/s. The detailed information of four grid systems is shown in Table 2, the mesh number of the left part was the same as that of the right part, and the mesh of middle part was refined as the fire existed in each grid system. When the combustion reaches quasi-stable state, the simulation results are shown in Figure 2. Figure 2 indicates that as the mesh number increases, the temperature values between grid systems 3 and 4 are closest with an error of less than 5 %. Considering the economical efficiency of computing time, grid system 3, with a total mesh number of 975,000, was deemed as the most suitable meshing scheme for numerical simulation.

Table 2. Specific parameters of the grid system.

Grid system	Region	Mesh number			Mesh size			Total mesh number
		X	Y	Z	ΔX	ΔY	ΔZ	
1	L	300	50	10	0.02	0.02	0.025	425,000
	M	250	50	10	0.012	0.02	0.025	
	R	300	50	10	0.02	0.02	0.025	
2	L	300	80	10	0.02	0.0125	0.025	720,000
	M	300	80	10	0.01	0.0125	0.025	
	R	300	80	10	0.02	0.0125	0.025	
3	L	300	50	20	0.02	0.02	0.0125	975,000
	M	375	50	20	0.008	0.02	0.0125	
	R	300	50	20	0.02	0.02	0.0125	
4	L	300	80	20	0.02	0.0125	0.0125	1,920,000
	M	600	80	20	0.005	0.0125	0.0125	
	R	300	80	20	0.02	0.0125	0.0125	
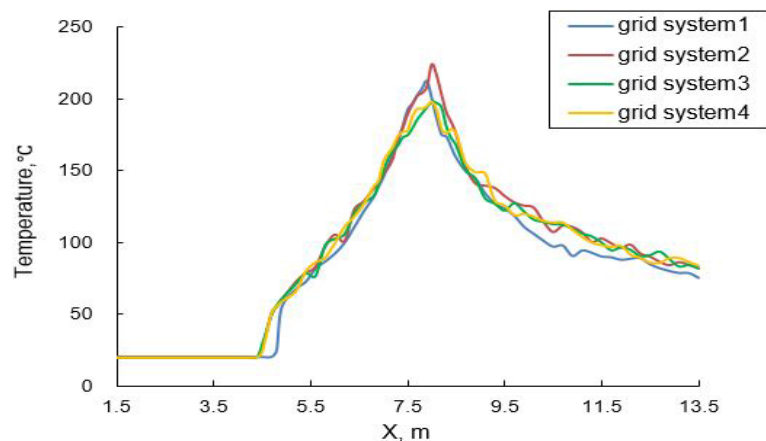
Figure 2. Temperature distribution of different grid systems along the *X* direction.

Zhang, Q., Pei, G.

2.4. Convergence of simulation

The Courant- Friedrichs-Lewy (CFL) criterion was applied to justify the convergence of the CFD simulation. The criterion plays a significant role in large-scale calculations in FDS. The calculated velocities were examined at each time step to follow the CFL constraint [18,19]:

$$\text{CFL} = \delta t \cdot \max\left(\frac{|u_{ijk}|}{\delta x}, \frac{|v_{ijk}|}{\delta y}, \frac{|w_{ijk}|}{\delta z}\right) < 1. \tag{8}$$

The initial time step is normally set automatically in FDS by dividing the size of a mesh cell by the characteristic velocity of the flow. During the calculation, the time step is varying and constrained by the convective and diffusive transport speeds to ensure that the CFL condition is satisfied at each time step. Figure 3 suggests that the CFL numbers during the iterations are in the range of 0.42 to 0.99, the CFL convergence criterion is satisfied because all of CFL numbers are less than the criteria value of 1. As seen in Figure 4, the time step eventually changes into a quasi-steady value with an average value of approximately 0.003 s when the fire reaches a quasi-steady state.
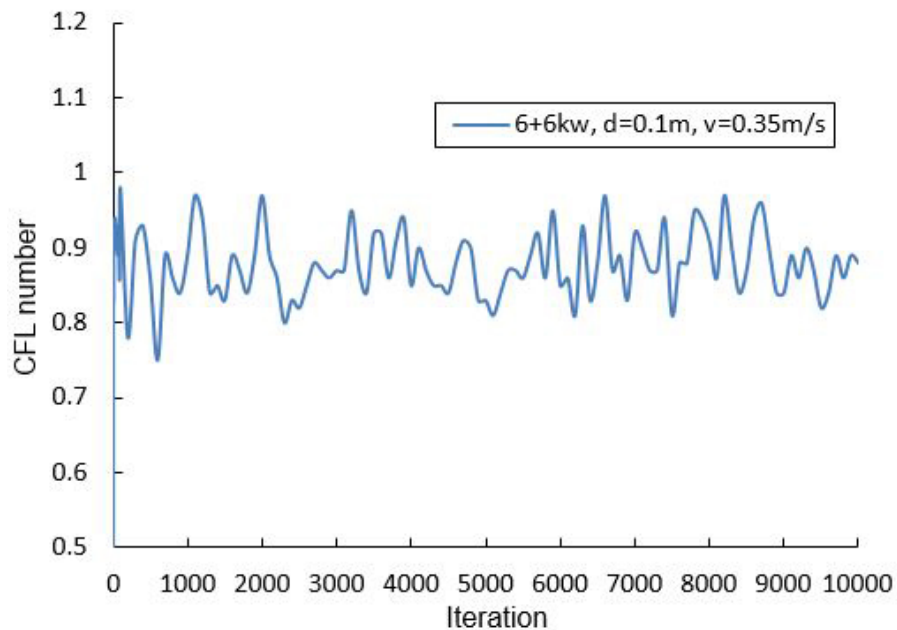

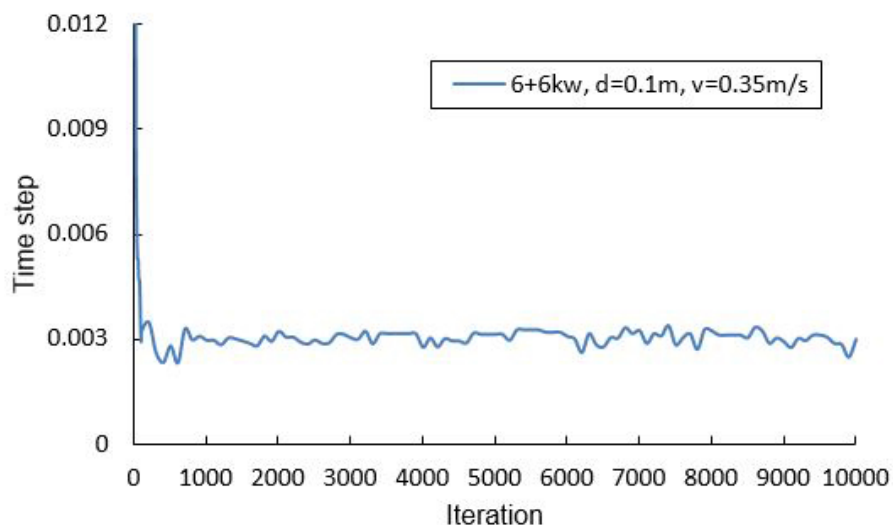**Figure 3. CFL number for FDS numerical simulation.**

Figure 4. Time step for FDS numerical simulation.

2.5. Comparison with experiments

Wu and Bakar [7] implemented many experiments in five tunnels of 15 m length with different cross-section shapes to study the critical velocity on the basis of the small-scale method. The experimental data in

tunnel D with dimensions 15×1×0.25 m were selected to prove the ability and reliability of the FDS model. In tunnel D, the burner was placed on the floor surface of the tunnel center, and the smoke temperature under the ceiling was detected by K-type thermocouples of diameter 0.25 mm. In order to detect the smoke temperature in the FDS model, thermocouples with an interval of 0.1 m were uniformly arranged below the top of the model tunnel centerline, the length ranged from 3.5 m to 11.5 m in the x direction, as shown in Figure 5. When the smoke flow approaches the quasi-steady state in the case of longitudinal ventilation, only the temperature of thermocouples located upstream of the fire source is close to the ambient temperature of 20 °C, at this time, the ventilation velocity is regarded as the critical ventilation velocity, as shown in Figure 6. As can be seen from Figure 7, the experimental and simulation values for critical velocity have the identical trend with minor error. Therefore, the FDS model can be used to study the critical velocity in tunnel fires.
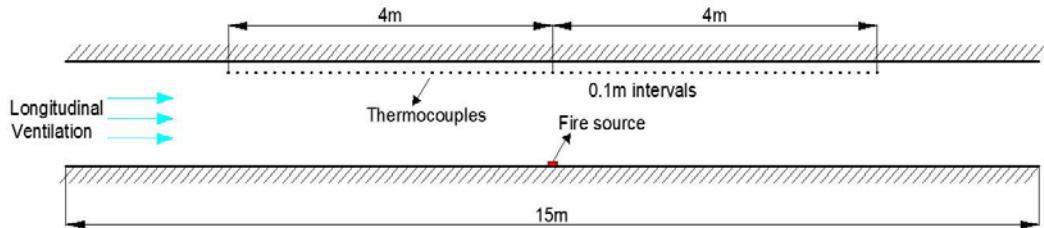

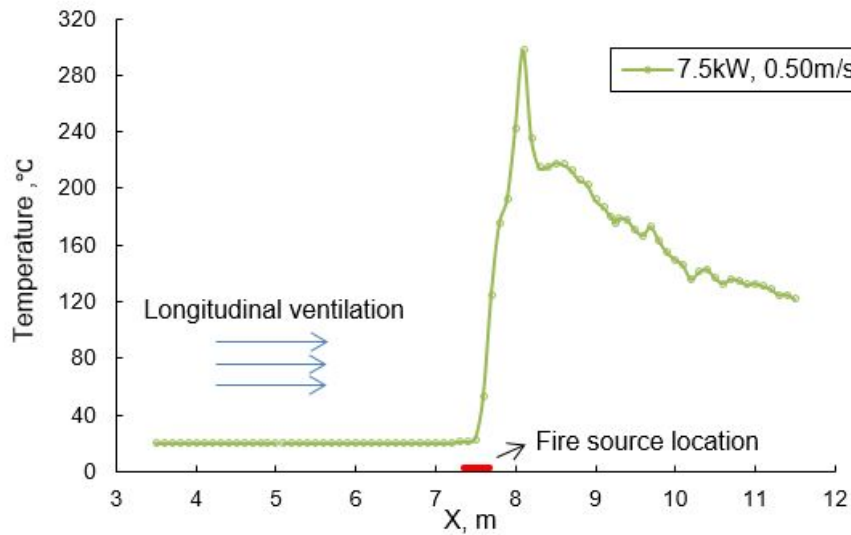Figure 5. Layout of thermocouples in the FDS simulation for the validation.

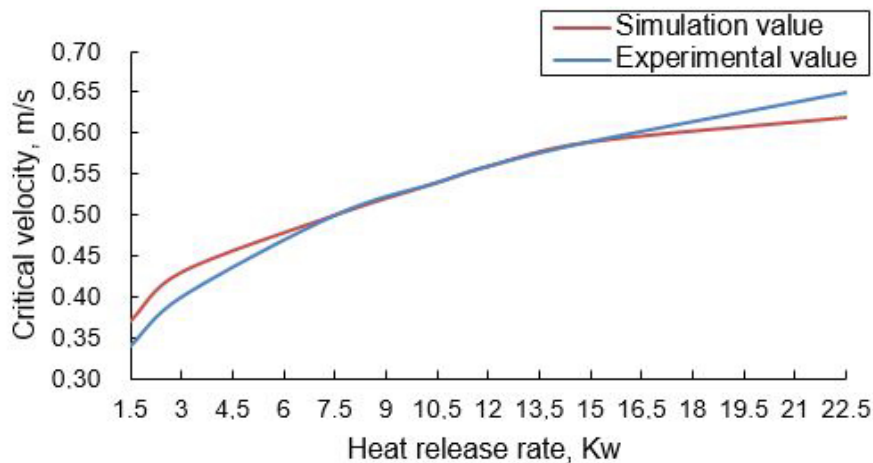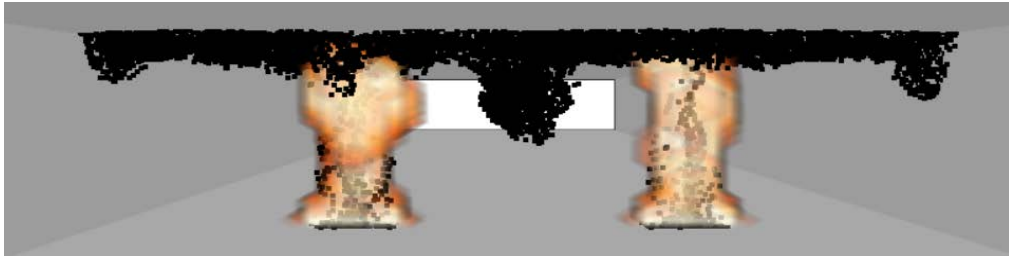Figure 6. Smoke temperature with critical ventilation velocity.

Figure 7. Comparison between the simulation values and experimental values
in Wu and Bakar's study for critical ventilation velocity.

3. Results and Discussion

Figure 8. Schematic diagram of smoke flow at the junction between double fires.

Tracer particles were added to observe the situation because of the low carbon content of methane. In Figure 8, without longitudinal ventilation velocity, the smoke spreads freely to both sides in the transverse direction of the tunnel, and there is a distinct convection bonding part when the smoke of horizontal diffusion from the double fires meets.
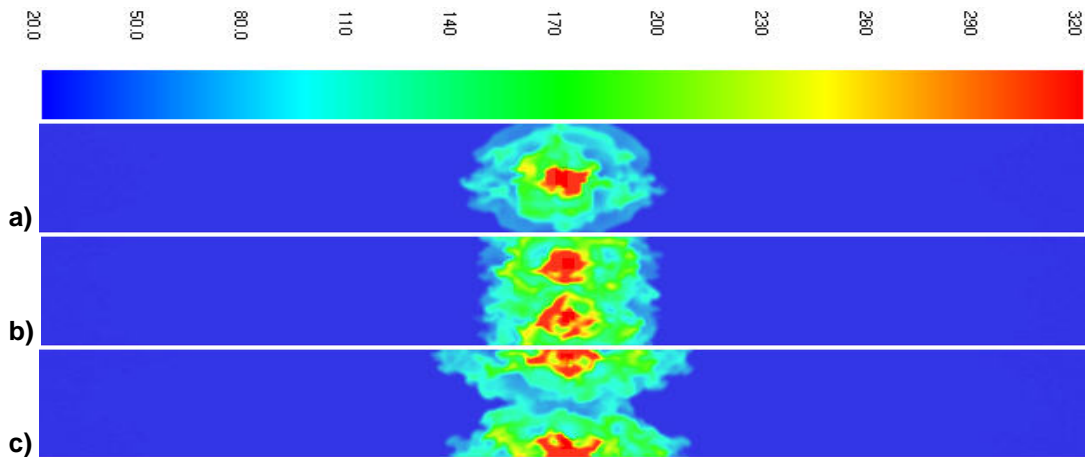
Figure 9. Temperature distribution of smoke (v = 0 m/s, t = 2 s) at d = (a) 0 m, (b) 0.4 m, and (c) 0.7 m.

In Figure 9, the temperature distribution is used to represent the smoke flow. From Figure 9 (a) to (c), when the distance between the two fires increases, the smoke length near the sidewall gradually increases and the smoke length in the centerline dwindles, thus, smoke flow is affected not only by buoyant force, but also simultaneously by the shear stress of the wall.
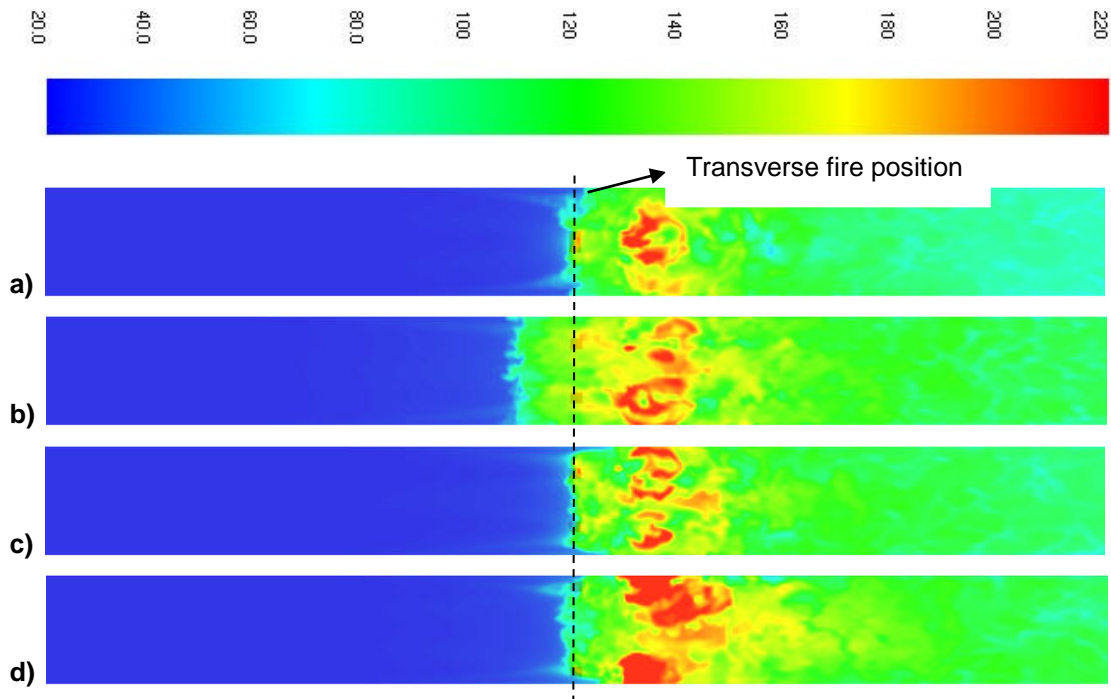
Figure 10. Temperature distribution of smoke (t = 70 s) at (a) d = 0 m, v = 0.56 m/s; (b) d = 0.4 m, v = 0.56 m/s; (c) d = 0.4 m, v = 0.60 m/s; and (d) d = 0.7 m, v = 0.56 m/s.

The temperature distributions under the quasi-stable state affected by different longitudinal ventilation velocities and different distances of double fire sources are shown in Figure 10. It is observed that the smoke back-layering length is 0 m when the longitudinal ventilation velocity is 0.56 m/s in Figures 10(a) and (d), which means that the longitudinal ventilation velocity is the critical velocity in these two conditions. However, as shown in Figure 10(b), smoke obviously lies at upstream of the fire sources under the same longitudinal velocity, but the upwind smoke is eliminated when the longitudinal ventilation velocity reaches to 0.6 m/s, so the critical velocity is not the same when the distance between double fires is different.
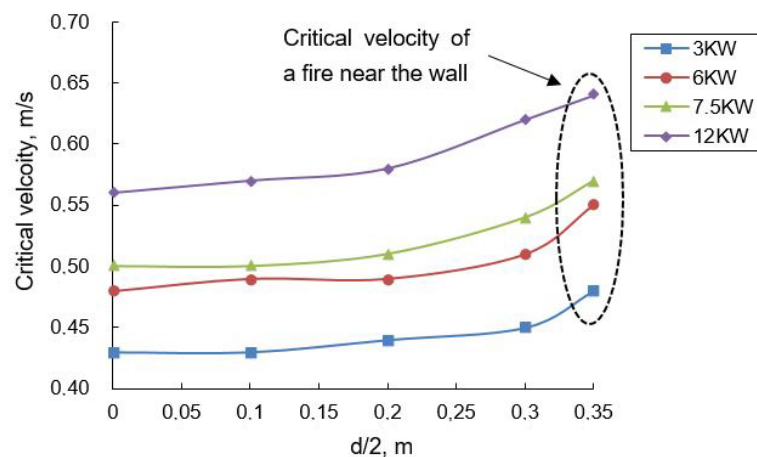
Table 3. Critical velocity of a single fire.

Heat release rate		Critical velocity, m/s				
		$d/2 = 0$ m	$d/2 = 0.1$ m	$d/2 = 0.2$ m	$d/2 = 0.3$ m	$d/2 = 0.35$ m
Single fire	Case (a): 3 kW	0.43	0.43	0.44	0.45	0.48
	Case (b): 6 kW	0.48	0.49	0.49	0.51	0.55
	Case (c): 7.5 kW	0.50	0.50	0.51	0.54	0.57
	Case (d): 12 kW	0.56	0.57	0.58	0.62	0.64
	24 kW	0.64	–	–	–	–

Table 4. Critical velocity of double fires.

| Heat release rate		Critical velocity, m/s							
		$d = 0$ m	$d = 0.1$ m	$d = 0.2$ m	$d = 0.3$ m	$d = 0.4$ m	$d = 0.5$ m	$d = 0.6$ m	$d = 0.7$ m
Double fires	Case (1) : 3 + 3 kW	0.48	0.47	0.50	0.53	0.52	0.51	0.50	0.48
	Case (2) : 6 + 6 kW	0.56	0.54	0.57	0.61	0.60	0.59	0.58	0.56
	Case (3): 7.5 + 7.5 kW	0.59	0.57	0.60	0.63	0.62	0.61	0.60	0.59
	Case (4): 12 + 12 kW	0.64	0.62	0.65	0.68	0.66	0.65	0.64	0.66

As shown in Tables 3 and 4, when the heat release rate of a single fire is equal to the sum of that of adjacent double fires, the critical velocity for double fires adjacent to each other is equal to the critical velocity for the single fire. An increase of the transverse distance between the fires results in the critical velocity reaching a maximum value at $d = 0.3$ m. However, as two fires approach the walls, the critical velocity for which is approximately equal to that for double fires at $d = 0$ m. Between the case (1), case (2) and case (3), the critical velocity at $d = 0.7$ m is the same as that at $d = 0$ m. But in case (4), the critical velocity at $d = 0.7$ m is greater than that at $d = 0$ m, because the higher heat release rate, compared with other cases at $d = 0.7$ m, causes the interaction between the fire plumes force to still exist in the tunnel, therefore, greater inertia force is needed to overcome both the buoyant force and the shear stress of the sidewalls.

Figure 11. Critical velocity for a single fire at different locations from the tunnel center.

According to Figure 11, the critical velocity gradually grows as the distance between the single fire and the tunnel centerline increases. When the fire source is near the wall, the critical velocity increases obviously as the fire plume, limited by the wall, involves less air to result in a greater velocity for smoke front. By comparing Figures 11 and 12, it becomes apparent that the critical velocity for a single fire is obviously lower than that for double fires at $d = 0$, 0.4, 0.6, and 0.7 m, which suggests that the smoke movement for double fires is reinforced by both the buoyant force and the shear stress of the sidewalls in the tunnel, so a greater critical velocity is needed to prevent the upwind smoke.
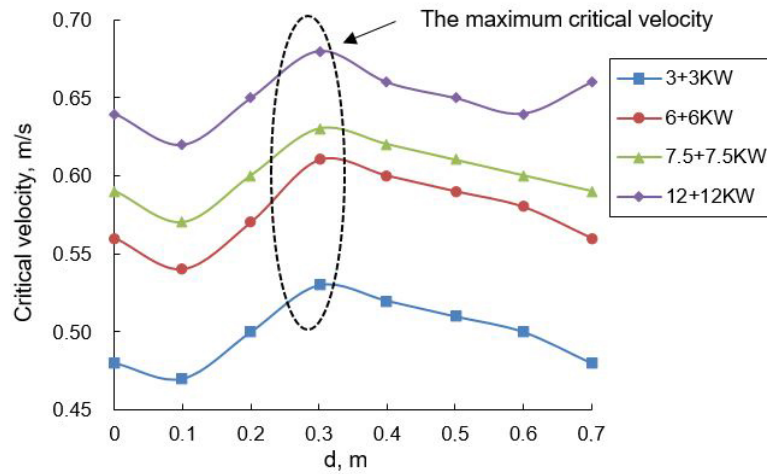
Figure 12. Critical velocity for double fires with different distances.

The simulated results show that the influence of distance between double fires on the critical velocity cannot be ignored. Therefore, the influence coefficient of distance was introduced as [21]:

$$a_i = \frac{\sum_{i=1}^{n}\left[(V^*_{double})_{i,j} / (V^*_{single})_j\right]}{n} \quad (i = 1, 2, 3, \ldots, n);$$

(9)

$$d^* = \frac{d}{H};$$

(10)

$$V^*_c = \frac{V_c}{\sqrt{g\bar{H}}},$$

(11)

where $(V^*_{single})_j$ is the dimensionless critical velocity at $d = 0$ m,

$(V^*_{doulbe})_{i,j}$ is the dimensionless critical velocity at $d > 0$ m,

i is the condition with different distances between double fire sources,

j is the condition with different cases,

d^* represents the dimensionless distance between double fire sources.

The relationship between $(V^*_{doulbe})_{i,j}$ and $(V^*_{single})_j$ is shown in Figure 13 when the data in Tables 3 and 4 are processed by Eq. (11).
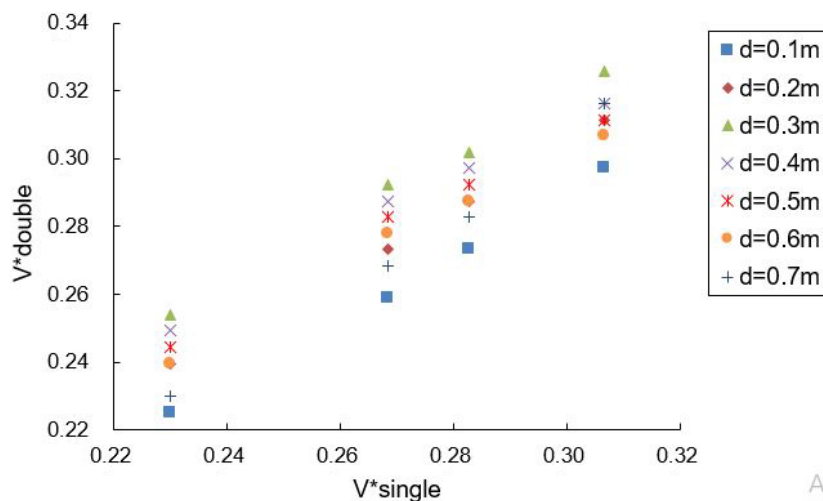
Figure 13. Comparisons of dimensionless critical velocity ($d > 0$ m) with dimensionless critical velocity ($d = 0$ m) for double fires.

Table 5. Relation between a_i and d^*.

d^*	0.25	0.50	0.75	1.00	1.25	1.50	.1.75
a_i	0.969	1.023	1.081	1.059	1.041	1.024	1.013
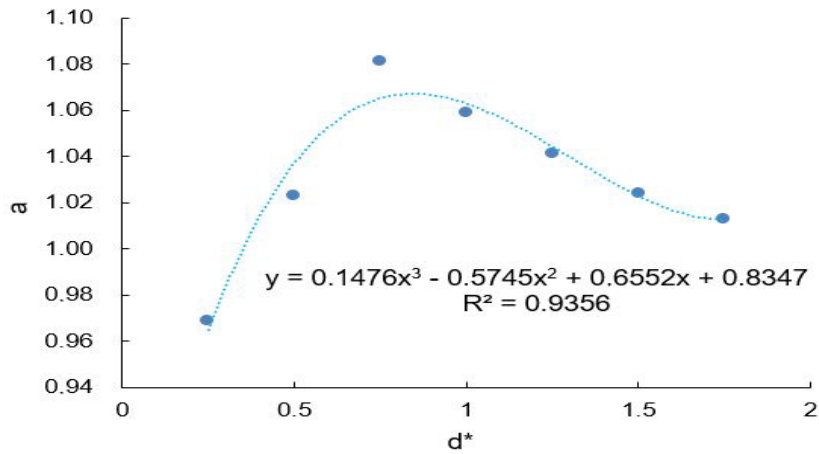
**Figure 14. Relationship between the influence coefficient of distance
and dimensionless distance for double fires.**

The relationship between a_i and d^* is shown in Table 5 and Figure 14. It is observed that a_i increases first and then decreases with increasing d^*. The following expression between a and d^* can be obtained by data fitting:

$$a = 0.1476d^{*3} - 0.5745d^{*2} + 0.6552d^* + 0.8347 \tag{12}$$

and so

$$(V^*_{doulbe})_{i,j} / (V^*_{\sin gle})_j = 0.1476d^{*3} - 0.5745d^{*2} + 0.6552d^* + 0.8347. \tag{13}$$

In order to validate the reliability of Eq. (13), the other two cases of fire combination were simulated using FDS. The detailed comparison results between the simulation values and predicted values by Eq. (13) are shown in Figures 15 and 16, it can be seen that the difference is small and the trend is essentially identical. Figure 17 shows that the basic situation of the tunnel model with dimensions 7×0.6×0.6 m, the tunnel hydraulic height was 0.6 m, the position of the 4.5 + 4.5 kw double fires was 2.5 m from the tunnel entrance longitudinally, and the distance between the double fires increased in the lateral direction [22]. Comparison of the simulation values in reference [22] with the predicted values by Eq. (13) is shown in Figure 18.
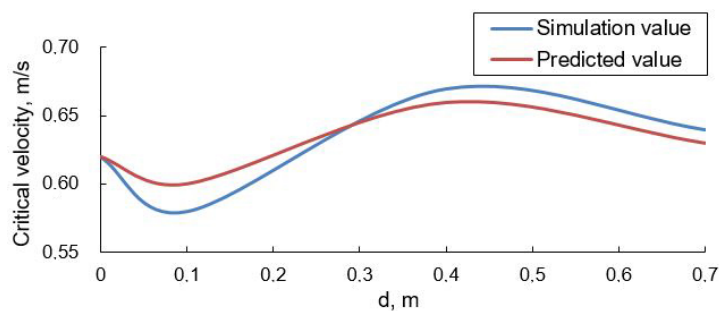
Figure 15. Critical velocity for 10 + 10 kw double fires.
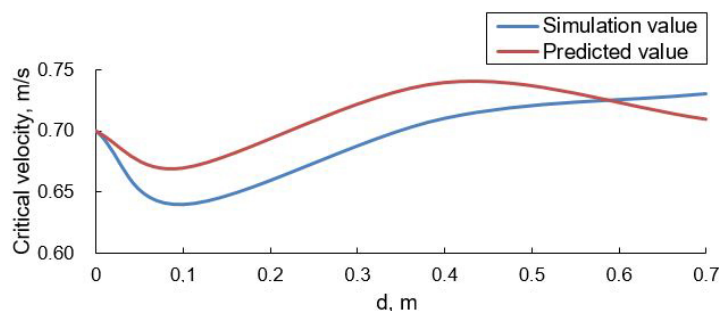
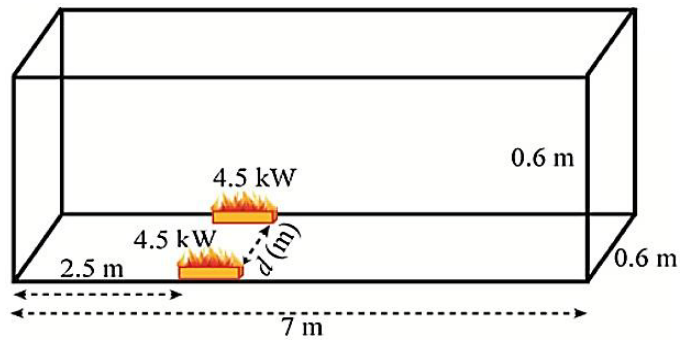**Figure 16. Critical velocity for 20 + 20 kw double fires.**

Zhang, Q., Pei, G.

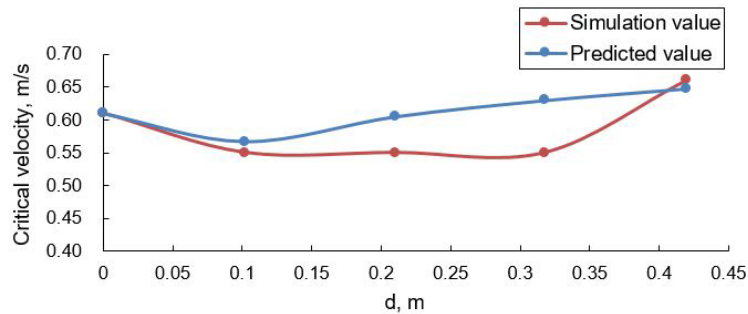**Figure 17. Diagram of the model tunnel [22].**

**Figure 18. Comparison between the predicted values by Eq. (13)
and the simulation values in reference [22].**

According to Figure 18, when the double fires are away from each other, the trend of prediction values by Eq. (13) first decreases and then increases gradually, and the trend of simulation values in reference [22] first decreases, then remains constant and eventually increases, there is a clear difference between the simulation values and predicted values at d = 0.32 m, but the difference is small at the other points. The difference results from the diverse cross-section geometry and the position of the double fire sources in the longitudinal direction, in addition, the prediction model was obtained under the condition with different fire combinations and different distances between the double fires, so the prediction model in this study is considered reliable for predicting the critical velocity for double fire sources.

4. Conclusions

In this study, a numerical investigation of critical ventilation velocity for transverse double fires in a tunnel was carried out using FDS 6.6.0. The same double fire sources were placed on the floor of the tunnel center and moved horizontally to the sidewalls, and the effect of different distances of the double fires on critical velocity was analysed. The main conclusions are as follows:

(1) The smoke movement for transverse double fires is affected by both the buoyant force and the shear stress of the sidewalls in the tunnel, greater inertia force is needed to overcome both the buoyant force and the shear stress of the sidewalls, so the higher critical ventilation velocity compared with a fire is needed to prevent upwind smoke.

(2) When double fires are completely placed next to each other, the critical velocity is equal to the state that a single fire by the sum of the heat release rate of the double fires is burned in the tunnel. The critical velocity for several fire combinations reaches the maximum value at d = 0.3 m as the transverse distance between double fires increases. Nevertheless, as double fire sources become close to the sidewalls, the critical velocity is approximately equal to the critical velocity for double fires at d = 0 m.

(3) Relations between the influence coefficient of distance and the dimensionless transverse distance as well as correlations between the critical ventilation velocity with and without distances for double fires were developed. The presented correlation can provide a reference value for smoke control and personnel evacuation in case of tunnel fire.

5. Acknowledgement

References

1. Vvedenskij, V.R., Gendler, S.G., Titova, T.S. Environmental impact of the tunnel construction. Magazine of Civil Engineering. 2018. No. 3. Pp. 140–149. DOI: 10.18720/MCE.79.15

Чжан Ц., Пэй Г.

2. Zhao, S., Liu, F., Wang, F., et al. A numerical study on smoke movement in a metro tunnel with a non-axisymmetric cross-section. Tunnelling and Underground Space Technology. 2018. Vol. 73. Pp. 187–202.

3. Li, Y.Z., Ingason, H. Effect of cross section on critical velocity in longitudinally ventilated tunnel fires. Fire Safety Journal, 2017.

4. Heselden, A., Hinkley, P. Smoke Travel in Shopping Malls Experiments in Co-Operation with Glasgow Fire Brigade–Part 1. Joint Fire Research Organization, Fire Research Note, 1970. Pp. 832.

5. Thomas, P.H. The Movement of Smoke in Horizontal Passages against Air Flow. Fire Research Technical Paper. 1963. Vol. 7. No. 1. Pp. 1–8.

6. Oka, Y., Atkinson, G.T. Control of smoke flow in tunnel fires. Fire Safety Journal, 1995. Vol. 25. No. 4. Pp. 305–322.

7. Wu, Y., Bakar M.Z.A. Control of smoke flow in tunnel fires using longitudinal ventilation systems – a study of the critical velocity. Fire Safety Journal, 2000. Vol. 35. No. 4. Pp. 363–390.

8. Li, Y.Z., Lei, B., Ingason, H. Study of critical velocity and backlayering length in longitudinally ventilated tunnel fires. Fire Safety Journal, 2010. Vol. 45. No. 6. Pp. 361–370.

9. Lee, Y.P., Tsai, K.C. Effect of vehicular blockage on critical ventilation velocity and tunnel fire behavior in longitudinally ventilated tunnels. Fire Safety Journal. 2012. Vol. 53. No. 10. Pp. 35-42.

10. Tang, W., Hu, L.H., Chen, L.F. Effect of blockage-fire distance on buoyancy driven back-layering length and critical velocity in a tunnel: An experimental investigation and global correlations. Applied Thermal Engineering. 2013. Vol. 60. No. 1-2. Pp. 7–14.

11. Gannouni, S., Maad, R.B. Numerical study of the effect of blockage on critical velocity and backlayering length in longitudinally ventilated tunnel fires. Tunnelling and Underground Space Technology. 2015. Vol. 48. Pp. 147–155.

12. Alva, W.U.R., Jomaas, G., Dederichs, A. The influence of vehicular obstacles on longitudinal ventilation control in tunnel fires. Fire Safety Journal. 2017. Vol. 87. Pp. 25–36.

13. Chow, W.K., Gao, Y., Zhao, J.H., et al. Smoke movement in tilted tunnel fires with longitudinal ventilation. Fire Safety Journal. 2015. Vol. 75. Pp. 14–22.

14. Yi, L., Xu, Q., Xu, Z., et al. An experimental study on critical velocity in sloping tunnel with longitudinal ventilation under fire. Tunnelling and Underground Space Technology. 2014. Vol. 43. Pp. 198–203.

15. Hu, L.H., Peng, W., Huo, R. Critical wind velocity for arresting upwind gas and smoke dispersion induced by near-wall fire in a road tunnel. Journal of Hazardous Materials. 2008. Vol. 150. No. 1. Pp. 68–75.

16. Zhong, W., Duanmu, W., Wang, T., et al. A Study of the Critical Velocity of Smoke Bifurcation Flow in Tunnel with Longitudinal Ventilation. Fire Technology. 2016. Vol. 53. No. 2. Pp. 1–19.

17. Wang, F., Wang, M. A computational study on effects of fire location on smoke movement in a road tunnel. Tunnelling & Underground Space Technology Incorporating Trenchless Technology Research. 2016. Vol. 51. Pp. 405–413.

18. McGrattan, K., Hostikka, S., McDermott, R., Floyd, J., Weinschenk, C., Overholt, K. Fire Dynamics Simulator Users' Guide (Version 6), NIST, Gaithersburg, MD, 2013a.

19. McGrattan, K., Hostikka, S., McDermott, R., Floyd, J., Weinschenk, C., Overholt, K. Fire Dynamics Simulator Technical Guide (Version 6), NIST, Gaithersburg, MD. 2013b.

20. Zadeh, S.E., Beji, T., Merci, B. Assessement of FDS 6 Simulation Results for a Large-Scale Ethanol Pool Fire. Combustion Science and Technology. 2016. Vol. 188. No. 4-5. Pp. 10.

21. Wei, Cun-xiang. Numerical simulation study on smoke exhaust effect of subway tunnel under multi-source fires. Safety engineering Institute, 2017.

22. Heidarinejad, G., Mapar, M., Pasdarshahri, H. A comprehensive study of two fire sources in a road tunnel: Considering different arrangement of obstacles. Tunnelling and Underground Space Technology. 2016. Vol. 59. Pp. 91–99.

Contacts:

Qiuyi Zhang, 0086+15228969340; luomusanchang@qq.com
Guihong Pei, 0086+15281073766; 570769297@qq.com